ACS OMEGA

Open Access

http://pubs.acs.org/journal/acsodf

Article

In Silico Analysis of the Aromaticity of Some *Carbo*-Metallabenzenes and *Carbo*-Dimetallabenzenes (*Carbo*-mers Proposed from Metallabenzenes)

David Arias-Olivares,* Andrés Becerra-Buitrago, Luis Carlos García-Sánchez, Diego V. Moreno, and Rafael Islas*

Cite This: *ACS Omega* 2024, 9, 10913−10928

Read Online

ACCESS | Metrics & More | Article Recommendations | Supporting Information

ABSTRACT: In the current work, we introduce a novel class of molecules termed *carbo*-metallabenzenes, and their aromaticity has been comprehensively analyzed. The molecules were strategically designed with the insertion of acetylene (C≡C or C_2) units in some selected metallabenzenes. Furthermore, if a second metallic unit is inserted (replacing a sp^2 carbon) in the *carbo*-metallabenzenes rings, a new family of *carbo*-mers is generated, and this second group has been named as *carbo*-dimetallabenzenes. The primary objective of this work is to ascertain, through various methodologies, whether these newly proposed molecules retain the aromatic characteristics observed in *carbo*-benzene. The methodologies employed for bond analysis and aromaticity exploration include the analysis of the molecular orbitals, energy decomposition analysis, electron density of delocalized bonds, magnetically induced current density, and the induced magnetic field ($\mathbf{B}^{ind}$). This study sheds light on that the insertion of the metallic centers reduces the electronic delocalization and their aromaticity is, in some cases, comparable with the electronic delocalization of the inorganic *iminobora*-borazine and also provides valuable insights into their electronic structure through a multifaceted analysis.

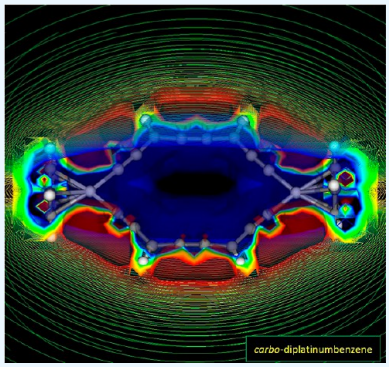

1. INTRODUCTION

In 1979, Thorn and Hoffmann proposed the theoretical existence of benzenes with one metal fragment instead one carbon (CH unit).[1] This kind of rings are stabilized by aromaticity, where the metal atom participates in the electronic delocalization. This proposal was followed by the synthesis of the first metallacycle in 1982: an osmabenzene.[2] Since then, the chemistry of metallacycles presented an enormous expansion and many other rings were synthesized with one metal center replacing a CH unit of benzene.[3] The two largest families of these compounds are osmabenzenes and iridabenzenes.[4] The electronic delocalization in rings containing metal atoms is catalogued as metallaromaticity[5] and, as mentioned before, is one of the mechanisms proposed for the stabilization of the rings.[6] The aromaticity of these rings has been computationally evaluated employing several methodologies, some of them based on the energetic stabilization such as isomer stabilization energy (ISE), proposed by Schleyer and Pühlhofer.[7] With this methodology, the electronic delocalization was computed in some platinabenzenes by De Proft and Geerlings in 2004.[8] Similarly, Lin et al. reported the synthesis and characterization of some rhenabenzenes, reporting the aromatic character of the rings employing ISE calculations.[9] Other methodologies dedicated to quantify/qualify the electronic delocalization are the magnetic-based indexes. The most employed index is NICS (nucleus independent chemical shifts) developed by Schleyer et al. in 1996. With NICS, the aromaticity of some metallacycles was analyzed.[10−14] Similar to NICS, the induced magnetic field ($\mathbf{B}^{ind}$) has been employed as

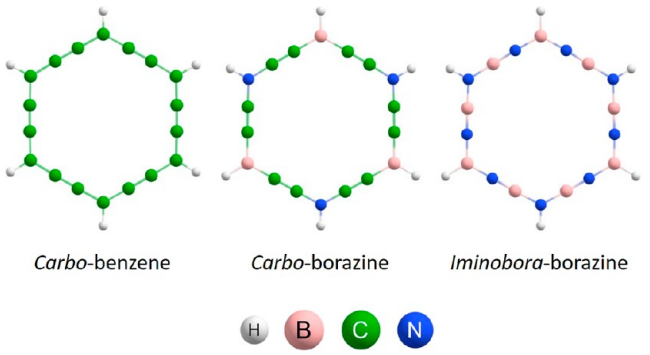

Figure 1. Structures of *carbo*-benzene, *carbo*-borazine, and *iminobora*-borazine.

Received: December 15, 2023
Revised: February 5, 2024
Accepted: February 8, 2024
Published: February 19, 2024

https://doi.org/10.1021/acsomega.3c10049
ACS Omega 2024, 9, 10913−10928

aromaticity's descriptor[15] and, with the B^{ind}, the diatropic character (associated with aromaticity) was determined in some metallacycles including some fused-cycles,[16] metal-laborazines,[17] and five-membered rings (5MR).[18,19] Finally, for a deeper appreciation of the metallacycle chemistry, some reviews are available.[3,6,20]

Additionally, *carbo*-mers are extended systems generated from the inclusion of one C≡C unit for each AB bond, forming A−C≡C−B bonds. If the number of the C≡C units, or C_2 units, incorporated is equal to the number of bonds, the molecular symmetry is not altered, but the AB length is increased.[21−23] With this methodology, the simplest example is acetylene, which is the *carbo*-mer proposed from the insertion of a C_2 unit in the H_2 molecule. In this line, the *carbo*-mer of benzene (C_6H_6) is called *carbo*-benzene ($C_{18}H_6$). Computational calculations show that *carbo*-benzene adopts a symmetric planar ring (D_{6h}), satisfying the structural criterion of aromatic compounds. For confirmation of the aromatic character, the aromaticity of *carbo*-benzene, carbo-borazine, the inorganic analogue *iminobora*-borazine, some *carbo*-cages, and *carbo*-C_4^{2+} (where C_4^{2+} is the analogue of the aromatic all-metal Al_4^{2-}) was studied in terms of the induced magnetic field.[24−26] See Figure 1 for *carbo*-benzene, *carbo*-borazine, and *iminobora*-borazine structures' representation. The aromaticity of other *carbo*-mers, with fused rings, such as *carbo*-azulene, has also been analyzed by Poater et al. in 2021.[27] Even more, 20 years ago, a set of *carbo*-mers of heterocycles had been studied, where included the parent system such as pyridine, phosphonine, furan, and pyrrol, among others, demonstrating that the aromaticity from the parent system is conserved after the *carbo*-merization.[28] Besides, aromaticity in *carbo*-mers is catalogued by Coqc et al. as *carbo*-aromaticity.[29] These types of calculations have inspired experimental chemists to work on its synthesis. Where the first attempts result in *carbo*-benzenes with various substitution patterns.[30,31] An experimental example of other types of extended systems is the germa[*N*]-pericycclyine, reported by Tanimoto et al. in 2017; where the authors synthesized and characterized a macrocycle composed by germanium and butadiyne units.[32] These previous works shed light to the theoretical-proposed derivates from *carbo*-benzenes as highly probable molecules to be studied and analyzed due to the conservation of their symmetry and their stability due to the electronic delocalization (aromatic character).

In the current work, *carbo*-mers generated from some selected metallabenzenes are computationally proposed. These new rings are called *carbo*-metallabenzenes. Also, if a second metallic center is incorporated, the new molecules are *carbo*-dimetallabenzenes. The aromaticity of *carbo*-metallabenzenes and *carbo*-dimetallabenzenes is analyzed as a possible mechanism of their stabilization.

2. COMPUTATIONAL DETAILS

The structures proposed for *carbo*-metallabenzenes were generated considering the incorporation of six C_2 units in some metallabenzenes following Scheme 1. In the second step, in the *carbo*-metallabenzenes proposed, a second metallic center was incorporated (replacing a sp^2 carbon of the **carbo**-metallabenzene), generating a new set of molecules named *carbo*-dimetallabenzenes (Scheme 2). In this paper, the positions of the metallic centers in *carbo*-dimetallabenzenes were referred with the prefixes 1,4-, 1,7-, and 1,10-positions, being 1 the position of the first metal atom, and the second

Scheme 1. Design of the *Carbo*-Metallabenzenes[a]

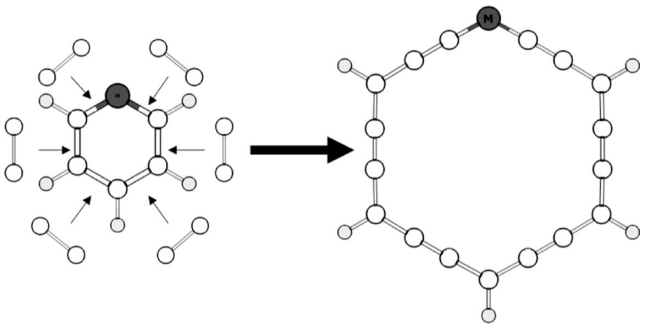

[a]White, gray, and black represent carbon, hydrogen, and metal atoms (including their ligands), respectively.

Scheme 2. Geometries Proposed for *Carbo*-Dimetallabenzenes; (A) Numbering Positions in the Carbo-Ring; (B) 1,4-Position, (C) 1,7-Position, and (D) 1,10-Position[a]

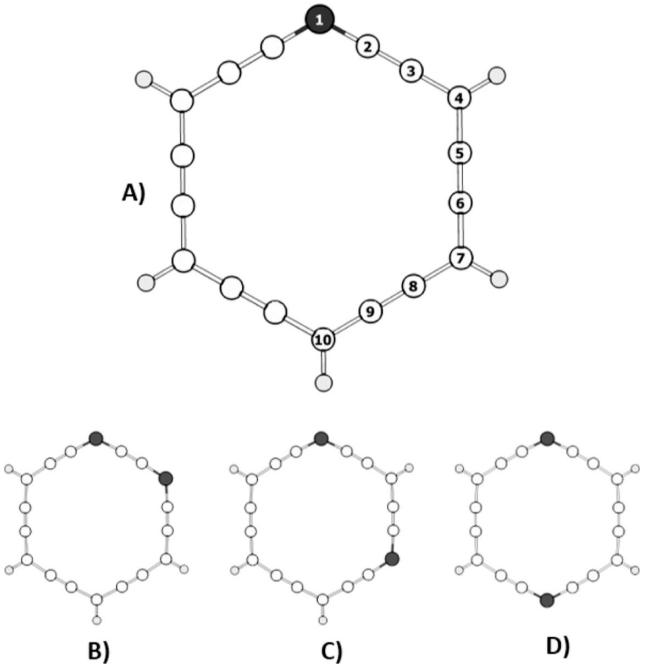

[a]The white and light-gray atoms represent carbon and hydrogen atoms. Black spheres represent the metallic centers M (where M = metal atoms and their respective ligands).

number (4, 7, or 10) the position of the second metallic atom as it is depicted in Scheme 2. All the geometries were optimized with the functional PBE0[33−35] employing the TZVP basis set[36] for all atoms, except the metal, where the SARC-ZORA-TZVP basis set[37] was used, in the program ORCA 5.0[38,39] and they were minima on their respective potential energy surfaces (PESs).

For EDA, MO construction was based on the ML fragments (metal with its ligands) and the rings (see Scheme 3), which helps to understand the interaction between the fragments through an analysis of bonding energies, combining a fragmented approach to the molecular structure with the decomposition of the interaction energy between fragments according to the Morokuma−Ziegler scheme [energy decom-

https://doi.org/10.1021/acsomega.3c10049
ACS Omega 2024, 9, 10913−10928

Scheme 3. Fragments Considered in EDA Calculations[a]

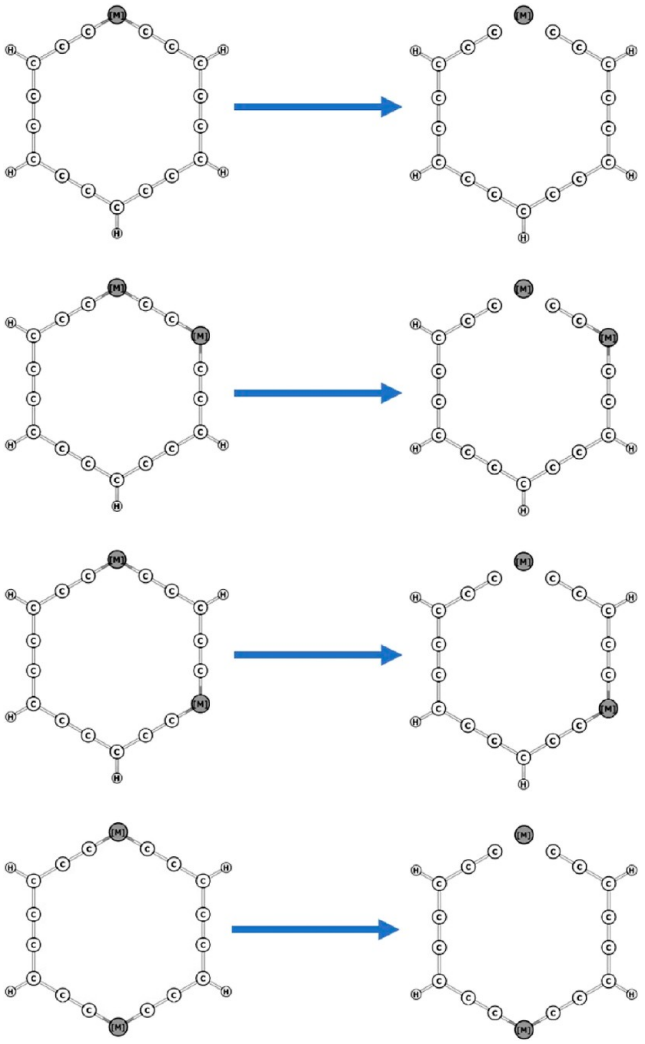

[a][M] represent metal atoms and the respective ligands.

position analysis (EDA) decomposition scheme]. This interaction between fragments is decomposed as follows

$$\Delta E_{\mathrm{Int}} = \Delta E_{\mathrm{Pau}} + \Delta E_{\mathrm{Ele}} + \Delta E_{\mathrm{Orb}} + \Delta E_{\mathrm{Dis}}$$

where ΔE_{Pau}, ΔE_{Ele}, ΔE_{Orb}, and ΔE_{Dis} represent the Pauli repulsion, electrostatic interaction, orbital-mixing terms, and dispersion correction, respectively.[40,41]

The electron density of delocalized bonds (EDDBs) function was implemented following the original methodology by Szczepanik et al.[42] The wave function was obtained at the same level of theory as the optimization, except for the metal atom, where the LANL2Z basis set[43,44] was used instead of the SARC-ZORA-TZVP in the Gaussian16 Rev. B.01 package.[45]

The magnetically induced current density (MICD),[46] which is related to aromatic response, was calculated using the linear response function[47] and the perturbing operator for the magnetic field. The MICD was plotted in the streamline representation of the current density using PyNGL[48] and was computed in DIRAC 17[49] at the DFT level of theory with the PBE0 functional.[35] The four-component Dirac-Coulomb Hamiltonian has been used alongside the unrestricted kinetic balance.[50] The cc-pVDZ basis set was employed for all atoms, except for metal atoms.[51] For the latter, the uncontracted and special Dyall double-ζ basis set was employed.[52]

The shielding tensors (σ) were computed in the program Gaussian 16 Rev. B.01 employing the PBE0 functional and def2-TZVP basis set,[53] including pseudopotentials for metal atoms.[54] The basis set and pseudopotentials were downloaded from Basis Set Exchange Web site.[55] The induced magnetic field can be computed following the equation $\mathbf{B}^{\mathrm{ind}} = -\sigma\mathbf{B}^{\mathrm{ext}}$, where $\mathbf{B}^{\mathrm{ext}}$ represents the external magnetic field applied on the perpendicular direction to the molecular plane, and σ represents the shielding tensor (second-rank tensor) computed in any point in the space.[15]

3. RESULTS AND DISCUSSION

3.1. Structural Results. *3.1.1. Carbo-Metallabenzenes.* For structural comparison, ethane, ethene, ethine, and *carbo*-

Scheme 4. Bond Lengths of Single, Double, and Triple Carbon−Carbon Bonds[a]

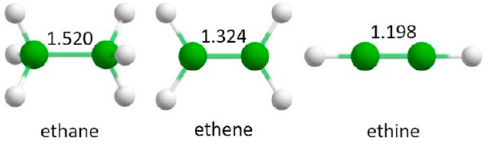

[a]Units are Å.

Scheme 5. CC Bonds Lengths in *Carbo*-Benzene[a]

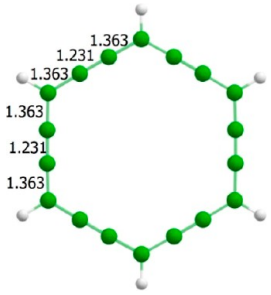

[a]Units are Å.

benzene geometries were optimized with the same level of theory employed in the optimization of the *carbo*-rings (Computational Details section). The geometries and the bond length distances are depicted in Scheme 4.

In the same line, *carbo*-benzene was optimized with the PBE0 functional and def2-TZVP basis set.[53] The bond lengths of (aromatic) *carbo*-benzene are depicted in Scheme 5. With these references, the first electronic delocalization inspection was possible. The triple bond of the C_2 units was not delocalized and shortens the bond length distance similar to the bond length observed in ethine.

The geometries of the rings containing one metallic fragment were optimized and they are depicted in Figure 2. On the first examination, the organic part of the *carbo*-metallabenzenes was compared to *carbo*-benzene's bond lengths: there was an alternation between triple and double bond lengths. For all the systems, the C_2 units inserted maintained the bond lengths associated with the carbon triple bond; the range observed was 1.227−1.234 Å, very similar to those observed in *carbo*-benzene (1.231 Å) and larger than methine (1.198 Å). The other C−C bond lengths lied on the range of 1.360−1.371 Å that could be associated with a

https://doi.org/10.1021/acsomega.3c10049
ACS Omega 2024, 9, 10913−10928

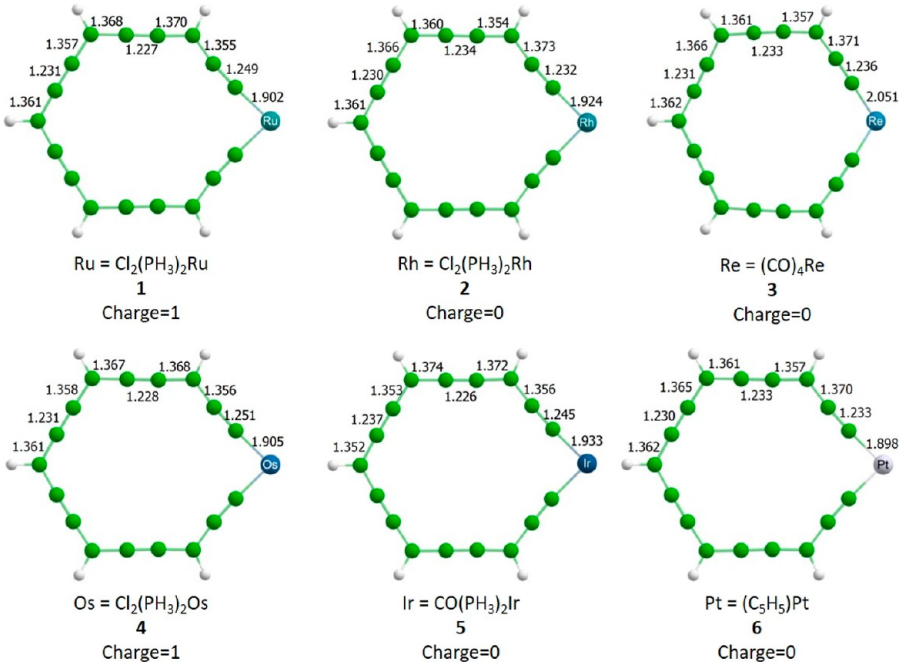

Figure 2. Bond lengths of *carbo*-metallabenzenes (Å). Green and white spheres represent carbon and hydrogen atoms, respectively. Ligands were removed for a better appreciation of the molecular rings. The value charge is the charge of the complete molecule.

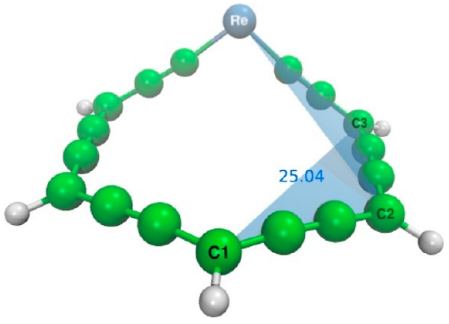

Figure 3. Dihedral angle formed with C1−C2−C3-Re of **3** is reported in degrees. White, green, and red spheres represent hydrogen, carbon, and oxygen atoms, respectively.

carbon−carbon double bond (1.324 Å). In few words, these *carbo*-mers were structurally comparable to *carbo*-benzene. Additionally, all the optimized structures, except **3** (see Figure 3), were planar rings. This nonplanar ring, adopted a bent structure; this type of geometries (bent rings) has been revised and discussed in metallabenzenes and heterometallabenzenes.[56,57] The electronic delocalization of all the planar systems was analyzed (vide infra).

3.1.2. Carbo-Dimetallabenzenes. As mentioned in the Computational Details section, *carbo*-dimetallabenzenes were proposed after a second CH unit of the *carbo*-metallabenzenes was replaced by a second metallic center. With this substitution, a new set of molecules were generated and analyzed. For convenience, the prefixes 1,4-, 1,7-, and 1,10- were employed in these rings. Three subgroups were generated based on the orientation of the metallic centers (Scheme 2). Only homodimetallabenzenes were proposed: *carbo*-diosmabenzene, *carbo*-dirutheniabenzene, *carbo*-diiridabenzene, *carbo*-dirheniumbenzene, *carbo*-dirhodiumbenzene, and *carbo*-diplatinabenzene.

The first subgroup, 1,4-*carbo*-mers were proposed with two metallic centers in nearest-neighbor vertices of the *carbo*-metallacycles. The system of rhodium and rhenium showed no minima on their respective PESs and, consequently, they were not reported in this section. The other four metallic centers (Ru, Os, Ir, and Pt) are depicted in Figure 4. As per the initial inspection, the presence of the C_2 units was visible through the bond lengths in agreement with the original *carbo*-benzene. However, the planarity was compromised by the vicinity of the voluminous metallic centers that include the metal atom and their respective ligands. For this reason, systems **8**, **9**, and **10**, could be catalogued as quasi-planar rings and this distortion was measured with dihedral angles reported in Figure 5.

Particularly, the optimized structure of **7** was a highly distorted ring (see Figure 5) and, consequently, electronic delocalization calculations were not realized in this carbomer. The rest of the rings, those that included osmium, iridium, and platinum, were quasi-planar rings. In these rings, bond length alternation was appreciable, but still comparable with *carbo*-benzene values (Figure 5).

In the second subgroup, the optimized geometries of 1,7-orientation *carbo*-dimetallabenzenes with ruthenium, rhodium, and rhenium (**11**, **12**, and **13**, respectively) were distorted rings. However, osmium, iridium, and platinum systems (**14**, **15**, and **16**, respectively) were planar rings, and they are depicted in Figure 6. In Figure 7, lateral views of **11**, **12**, and **13** are depicted for the appreciation of the distortion of the rings generated by the presence of the metallic centers. In **11**, the Ru atom did not form a part of the ring and, for consequently, the organic skeleton was a ring with 16 carbon atoms. In the other rings, the metallic centers were a part of the cyclic structures. The bond lengths of **11** were not different from those measured in **12**, **13**, **14**, **15**, and **16**; presenting similar lengths observed in *carbo*-benzene. The only difference of **11** was the C−C bond formed in the place where the C-metal-C bond was placed, forming a 16-carbon ring.

https://doi.org/10.1021/acsomega.3c10049
ACS Omega 2024, 9, 10913−10928

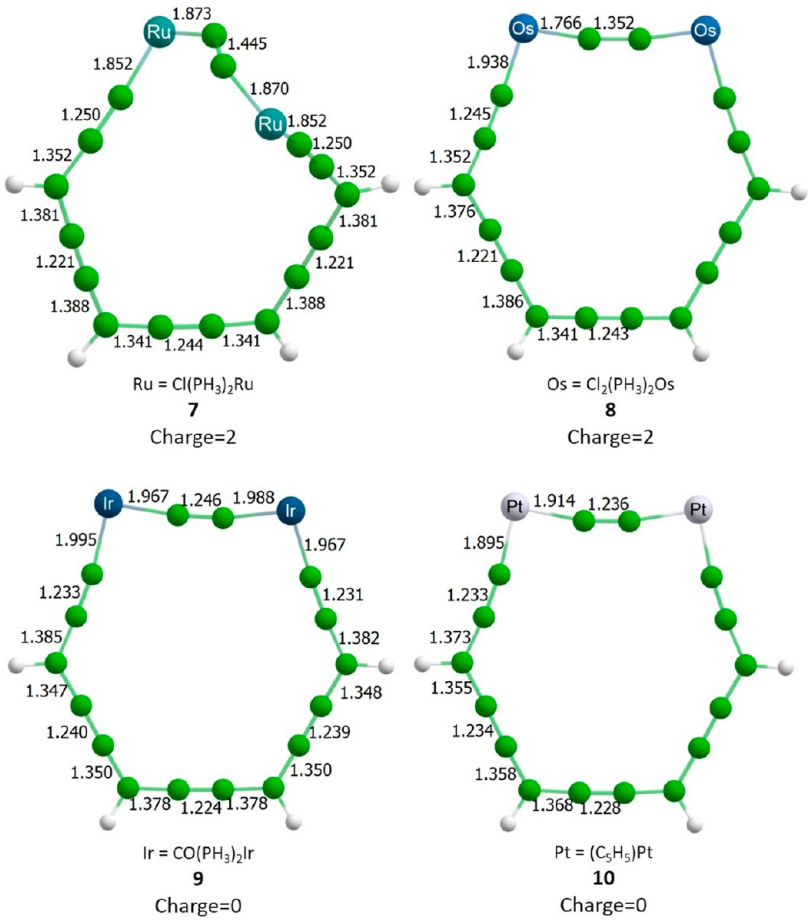

Figure 4. Bond lengths of 1,4-*carbo*-dimetallabenzenes. The units are Å. Green and white spheres represent carbon and hydrogen atoms, respectively. Ligands were removed for a better appreciation of the molecular rings. The value charge is the charge of the complete molecule.

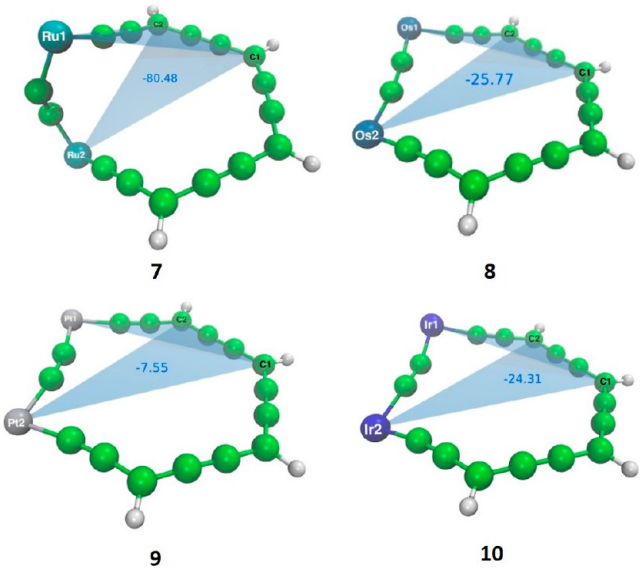

Figure 5. Some selected dihedral angles (C1−C2−M1−M2, where M1 = M2 = Ru, Os, Ir, and Pt) formed in **7**, **8**, **9**, and **10**. The units reported are degrees.

The third subgroup, with 1,10-orientation, the rings adopted a planar configuration except for the rhodium system, **18**; for this reason, this system was not considered for further analysis. The quasi-planar ring was **17** which presented a small deviation from planarity, adopting a flat boat. Other systems (**19**, **20**, **21**, and **22**) were completely planar rings. In Figure 8, the geometries and bond length distances are depicted, and in Figure 9, the distorted structure of **18** is shown.

3.2. Electronic Structure. *3.2.1. Molecular orbitals.* The analysis of the molecular orbitals (MOs) of all the molecules was realized, showing that not only the classic π-MO participated in the electronic delocalization, but the in-plane orbitals, which are related with triple bonds of acetylene units. In some cases, it was clear the radial nature of specific MOs. Nevertheless, these radial MO were mixed with the π-MO from the ring or the MO of the metal atoms (see Figure 10). This phenomenon was mentioned by Maraval and Chauvin; they explained it with the generation of homoconjugation to adjacent triple bonds (homoaromaticity), generated by the reduced gap between HOMO and LUMO, and this situation could be observed in extended heteroperycyclynes and expanded radialenes.[23] An example of homoconjugation is depicted in Figure 10. It is important to highlight that *carbo*-benzene is aromatic, but it is not homoaromatic.[28] Furthermore, it is possible that the $d_{x^2-y^2}$ atomic orbitals could favor the electronic delocalization process within the radial orbitals (π_{in_plane} orbitals) of the proposed systems. That situation is also observed in the system herein reported (see Figure 11). Therefore, the HOMO−LUMO gap was measured in our system and reported in Table 1. The computed value for the carbomer is 72.87 kcal/mol. Thus, a reduction in the HOMO−LUMO gap is observed in all systems. The trends

https://doi.org/10.1021/acsomega.3c10049
ACS Omega 2024, 9, 10913−10928

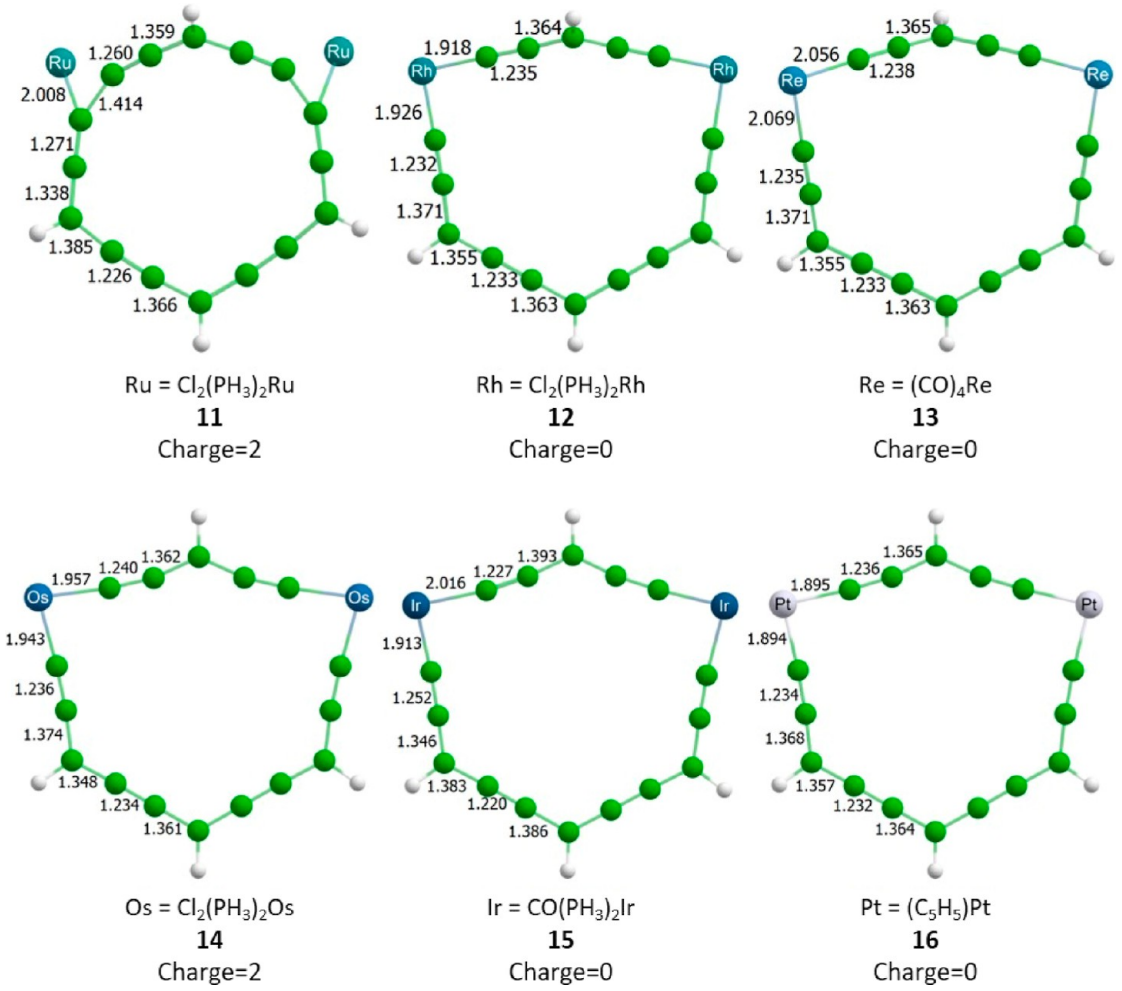

Figure 6. Bond lengths of *carbo*-dimetallabenzenes. The units are Å. Green and white spheres represent carbon and hydrogen atoms, respectively. Ligands were removed for a better appreciation of the molecular rings. The value charge is the charge of the complete molecule.

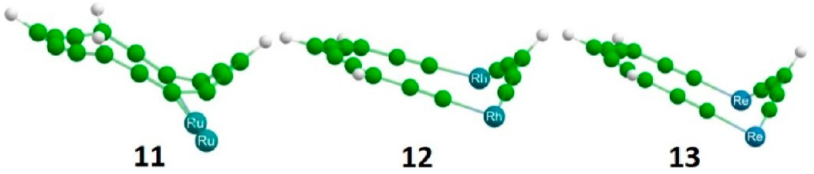

Figure 7. Lateral view of **11**, **12**, and **13**. The distortion of the rings was appreciable. Green and white spheres represent carbon and hydrogen atoms, respectively. Ligands of the metal centers were removed for a better appreciation of the molecular.

appears naturally if the gap is compared with the atomic mass of each metallic center. For the monosubstituted systems, the gap increase as the mass increase for the Ru−Rh−Re triad, as well as for Os−Ir−Pt triad. On the other hand, for the 1,4-substitution, the gaps decrease in the same triads. Even more, for the 1,7- and 1,10-substitution no evident trends arise; nevertheless, the Rh and Ir present the highest gaps for those substitutions, recalling that they belong to the same group in the periodic table.

A deeper analysis for the HOMO−LUMO gap was conducted based on the lack of correlation between the energy gap and the aromatic response that some systems have. Unfortunately, the analysis of in-plane HOMO−LUMO as well as the analysis of classical π-HOMO−LUMO gap is not conclusive, i.e., there is not a clear correlation among the (de)stabilization of the metal HOMO (in plane or perpendicular), and the type or lack of aromatic behavior. Nevertheless, the ratio of mixed p/d metal orbitals gives interesting results, if the d orbitals contribute with more than 50%, the molecules present a Hückel aromatic behavior, and on the contrary, if the p orbitals contribute with more than 50%, then the system exhibits a (double) Möbius aromatic character; unfortunately, the information is not enough to differentiate between the traditional Möbius or Double Möbius aromatic character.

Systems **3**, **7**, **12**, **13**, and **18** were excluded since they do not meet the planarity criteria. Also **11** was discarded since it does not contain the ML fragments within the ring. For these rings, only π-MO diagrams were analyzed and depicted in the Supporting Information.

For the remaining systems, classic π-MO and radial π-MO diagrams were constructed. Furthermore, the contribution of

https://doi.org/10.1021/acsomega.3c10049
ACS Omega 2024, 9, 10913−10928

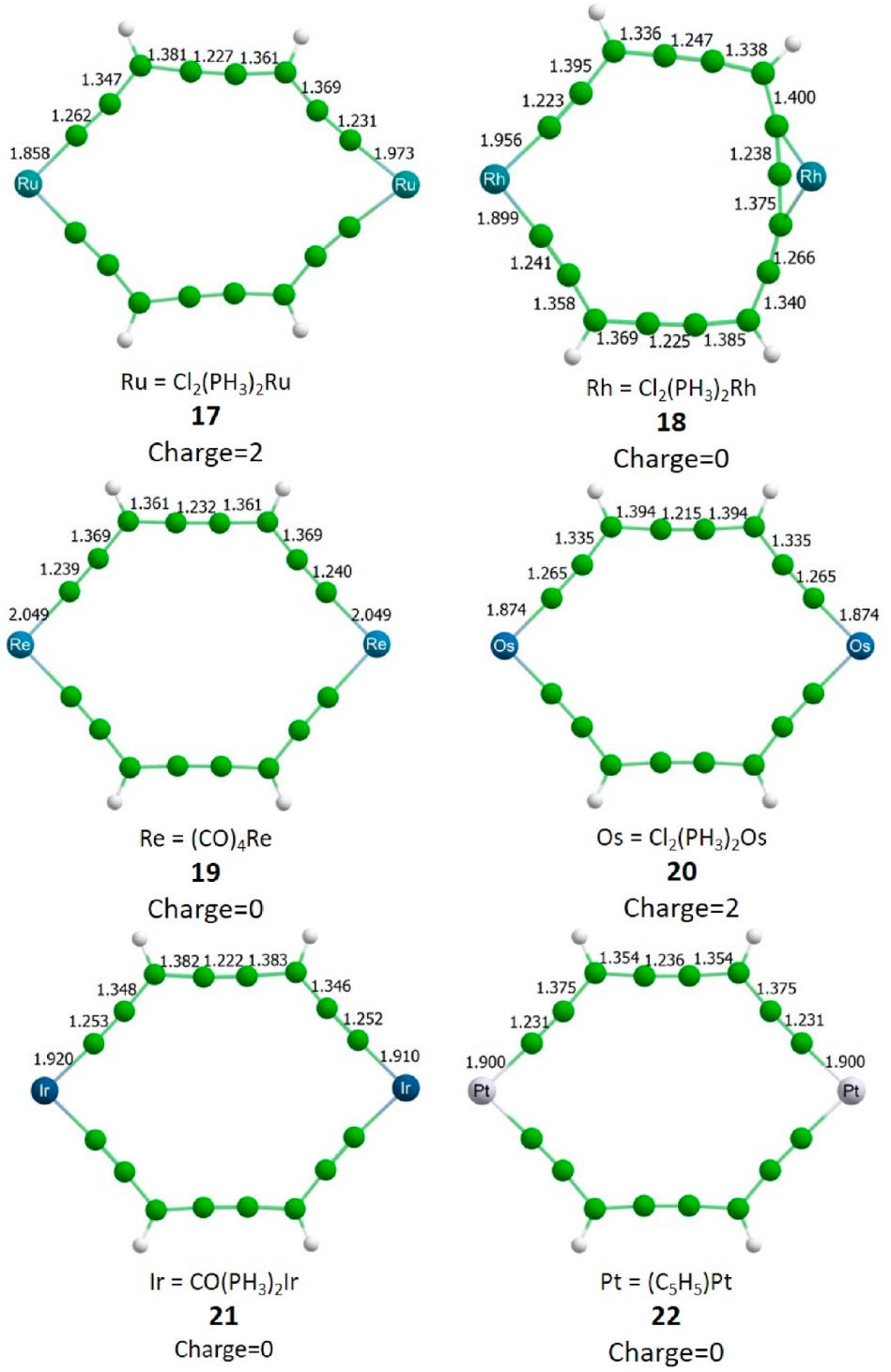

Figure 8. Bond lengths of *carbo*-dimetallabenzenes. The units are Å. Green and white spheres represent carbon and hydrogen atoms, respectively. Ligands were removed for a better appreciation of the molecular rings. The value charge is the charge of the complete molecule.

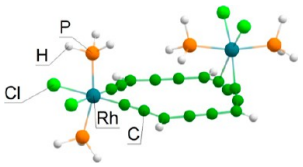

Figure 9. Distortion observed in **18**. One of the Ru centers was placed out of the ring and adopted a perpendicular position to the molecular plane.

the d_{yz} and d_{xz} orbitals made by the ML fragments for monosubstituted systems, and by the combination of ML−metalorganic fragments for double-substituted systems was analyzed, generating three types of aromaticity: Hückel, Möbius, and Double-Twisted Möbius (see Figure 12). Due to the construction of atomic orbitals based on symmetry, the 1,10-orientation rings were either Hückel or Double-Twisted Möbius.

The π electrons were counted considering the radial orbitals, to identify if the systems fulfill the number of electrons

https://doi.org/10.1021/acsomega.3c10049
ACS Omega 2024, 9, 10913−10928

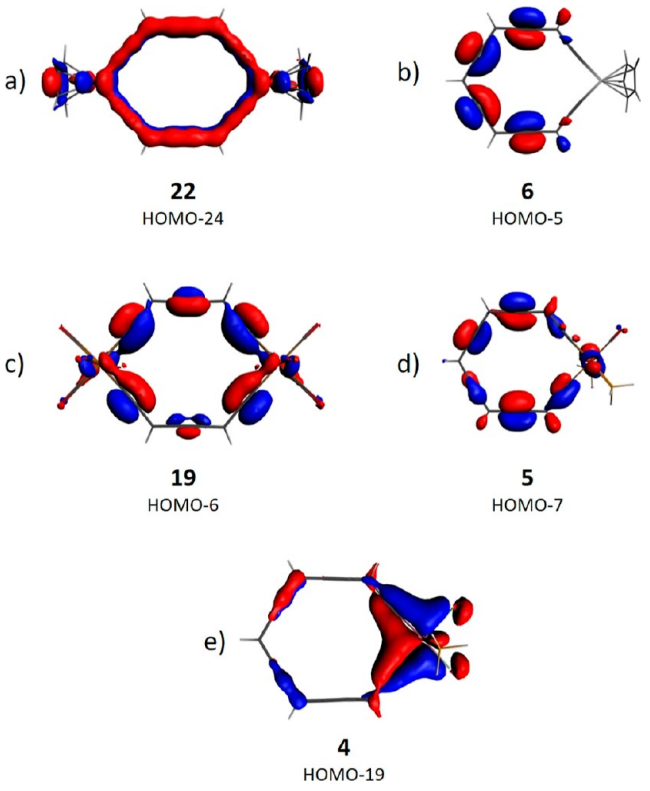

Figure 10. Examples of MOs: (a) HOMO − 24 of **22** represents the out-of-plane MO (π-MO), (b) HOMO − 5 of **6** represents the in-plane MO (radial-MO), (c) HOMO − 6 of **9** represents the orbital generated by the combination of the metal atom with the in-plane triple bond of the C_2 unit, (d) HOMO − 7 of **5** represents MOs that could be associated with a Möbius band, and finally, (e) is the HOMO − 19 of **4** and it represents the homoconjugation generated between the metal atom and the in-plane MOs of the adjacent carbon triple bonds.

required for each type of aromaticity. It was found that systems **4**, **5**, **9**, **15**, and **21** presented Hückel aromaticity ($4n + 2$) with $n = 10$ for all of them, except for **5**, which has $n = 8$. Systems **1**, **2**, **6**, **8**, and **16** could be associated with Möbius aromaticity ($4n$) with $n = 10$, 11, 9, 13, and 11, respectively. Systems **10**, **14**, **17**, **19**, and **22** were Double-Twisted Möbius Aromatic with $n = 11$, 12, 13, 9, and 10, respectively. System **20** was Double-Twisted Möbius antiaromatic since its electron count does not fit with the $4n + 2$ rule, proposed for the Double-Twisted Möbius systems,[58] as it has 48 π electrons between classic and radial π MO. We have analyzed the stability of the disubstituted isomers through relative energies obtained by single-point energy calculation and the aromatic behavior of each system has been related.

For the Os systems (**4**, **8**, **14**, and **20**), all of them exhibited a different aromatic character, i.e., system **4** (monosubstituted); system **8** (1,4-*carbo*-mer); and systems **14** and **20** (1,7- and 1,10-*carbo*-mer) could be classified as Hückel, Möbius, and Double-Twisted Möbius, respectively. Nevertheless, **20** presented an antiaromatic behavior; even more, all of them showed a low diatropic response. In Table 1, the relative energy of the *carbo*-dimetallabenzene isomers is also shown, and the least stability (higher ΔE) belongs to system **20**. It is in agreement with the electron counting and magnetic responses. The most stable isomer was the 1,4-oriented, being almost 20 kcal/mol more stable than the second most stable isomer.

For the Ir systems (**5**, **9**, **15**, and **21**), all of them were labeled as Hückel aromatic molecules. The most stable isomer was the 1,7-*carbo*-mer, but only by 3 kcal/mol.

For the Pt systems (**6**, **10**, **16**, and **22**), all of them exhibited Möbius or Double-Twisted Möbius aromatic character, i.e., systems **6** (monosubstituted) and **16** (1,7-*carbo*-mer); and systems **10** and **22** (1,4- and 1,10-*carbo*-mers) could be classified as Möbius and Double-Twisted Möbius, respectively. In coincidence with the iridium rings, the most stable isomer was the 1,7-*carbo*-mer.

3.2.2. Energy Decomposition Analysis. The analysis of the interaction of the metallic center with the ring of the proposed structures, were done with EDA, following the partition scheme proposed in computational details section: the interaction analyzed is between one of the metallic centers with the rest of the ring (see Scheme 3 in the Computational Details section).

The values of the EDA calculations are depicted in Table 2. For *carbo*-metallabenzenes, four out of six rings presented a dominant percentage of the electrostatic contribution to the interaction energy (% ΔE_{Elec}); on the other hand, only ruthenium and osmium rings presented a dominant orbital contribution (% ΔE_{Orb}).

Also, in Table 2, two different sets of E_{int} are observed, one who presented bigger orbital energy contribution which is related with covalent interaction and, the other one, with bigger electrostatic energy contribution which is related with ionic interaction. The former includes the systems **1**, **4**, **8**, **14**, **20**, and **17** which were taken into account for aromaticity studies, while the systems **7** and **11** were outside of the analysis due to lack of planarity. In this way, systems **1**, **4**, and **14** presented bigger orbital contributions (>60%), in agreement with the $\mathbf{B}^{ind}$ calculations (vide infra) that showed that these systems were the least diatropic. The latter were the systems **2**, **19**, **5**, **6**, **9**, **10**, **15**, **16**, **21**, and **22** with higher diatropic response in comparison with those that presented a higher orbital interaction; a possible explanation for this behavior was the diminished σ interaction between the metal and the nearest carbon but a higher electrostatic interaction among the axial p−d interaction through the long bond distances as observed in previous EDA analysis between metals and light atoms.[17] Furthermore, the interaction between the metal center and the ring was always in the range of −8.5 and −15.3 eV/mol. The highest interaction consistently remained in the Pt and Ir centers. Systems **3**, **12**, **18**, and **13**, have been outside of this analysis based on the planarity criteria.

3.2.3. Electron Density of Delocalized Bonds. Analyzing the ring and its delocalization, the $EDDB_P$ (electrons delocalized along a selected pathway) was used instead of the global descriptor ($EDDB_G$) or the description avoiding hydrogen atoms ($EDDB_H$). The inclusion of the ligands from the metal fragment introduced electron density around the metal and this expanded the visualized isosurface of EDDB, giving rise to misinterpretations over the electrons delocalized and their electron counting (Figure 13). This led to a different π-electron counting compared with the EDA analysis. Thus, for system **6**, the population of delocalized electrons in the $EDDB_G$ was 22.47e (1.79e from Pt), in the $EDDB_H$ was 20.92e (1.76e from Pt), and finally for $EDDB_P$ was 11.46e (0.37e from Pt).

Analogue to benzene, the *carbo*-benzene showed a fully delocalized bond over the system (Figure 14A). In most of the systems, similar delocalization was observed over the organic

https://doi.org/10.1021/acsomega.3c10049
ACS Omega 2024, 9, 10913−10928

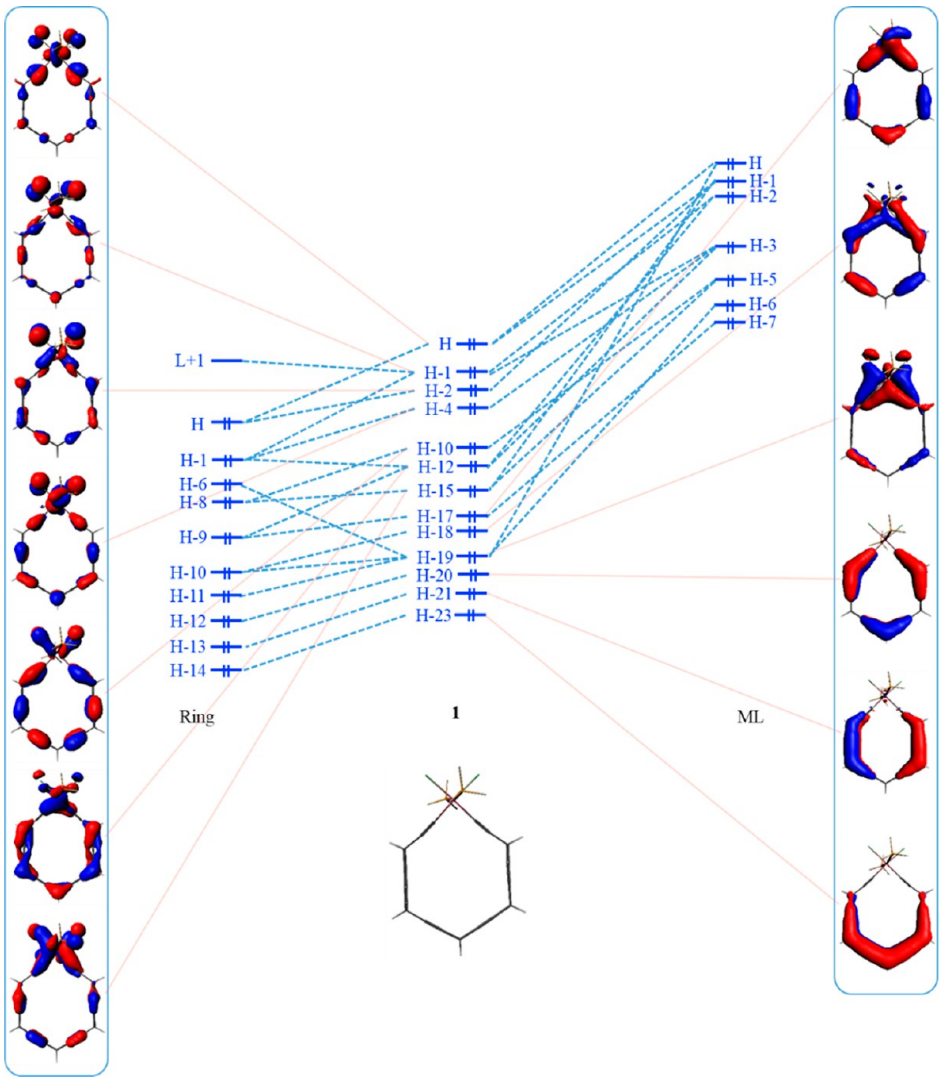

Figure 11. Qualitative MO diagram for *carbo*-rutheniabenzene. Only π electrons are depicted.

Table 1. Aromatic Character and Relative Energies for the Systems Containing Os, Ir, and Pt[a]

metal	system	substitution	aromaticity	character	ΔE (kcal/mol)	ΔE_{L-H} (kcal/mol)
Os	4	monosubstituted	Hückel	aromatic		28.56
	8	1,4-*carbo*-mer	Möbius	aromatic	0.00	47.03
	14	1,7-*carbo*-mer	Double-Twist Möbius	aromatic	19.57	31.78
	20	1,10-*carbo*-mer	Double-Twist Möbius	antiaromatic	26.47	9.77
Ir	5	monosubstituted	Huckel	aromatic		52.71
	9	1,4-*carbo*-mer	Huckel	aromatic	7.38	38.28
	15	1,7-*carbo*-mer	Huckel	aromatic	0.00	55.85
	21	1,10-*carbo*-mer	Huckel	aromatic	2.95	46.44
Pt	6	monosubstituted	Möbius	aromatic		48.53
	10	1,4-*carbo*-mer	Double-Twist Möbius	aromatic	15.23	31.81
	16	1,7-*carbo*-mer	Möbius	aromatic	0.00	48.08
	22	1,10-*carbo*-mer	Double-Twist Möbius	aromatic	8.09	29.41

[a]The relative energies were computed at the PBE0/TZVP level as it was reported in the section of Computational Details. The HOMO−LUMO gap is also reported in kcal/mol. The carbomer has a L−H gap of 72.87 kcal/mol.

fragments, and it slightly vanished close to the metal. As an example, the platinum systems were shown alongside *carbo*-benzene (Figure 14). This lack of homogeneous delocalization played an important role over the induced magnetic field avoiding a fully delocalized nature of the electron density but an induced current density in parts of the ring. Platinum always showed an electron contribution of d-like orbitals to the ring. Nevertheless, the contribution was not high enough to be fully delocalized. All EDDB plots are presented in ESI. While the *carbo*-benzene had a uniformly delocalized electron nature of 0.78e per atom (total 14.09e), all the proposed *carbo*-metallabenzenes contributed with less than 0.5e for metal

https://doi.org/10.1021/acsomega.3c10049
ACS Omega 2024, 9, 10913−10928

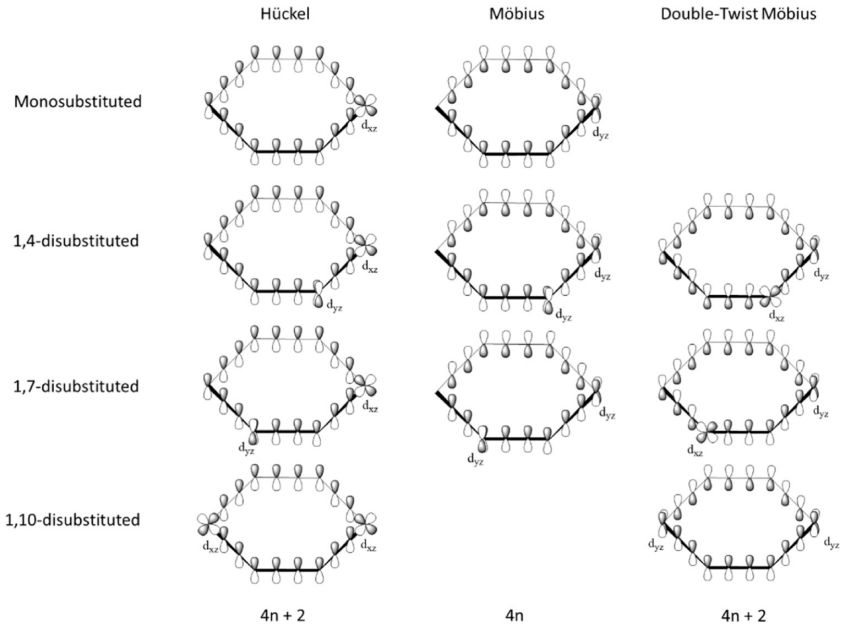

Figure 12. Types of aromaticity proposed for *carbo*-metallabenzenes and *carbo*-dimatellabenzenes.

Table 2. EDA Values Computed in All the Proposed Rings[a]

	system	metal	net charge	ML charge	ΔE_{Pauli}	ΔE_{Elec}	% ΔE_{Elec}	ΔE_{Orb}	% ΔE_{Orb}	ΔE_{Dis}	ΔE_{Tot}
carbo-metallabenzenes	1	Ru	1	0	15.86	−9.03	37.06	−15.33	62.94	−0.25	−8.76
	2	Rh	0	1	15.66	−16.90	61.26	−10.69	38.74	−0.30	−12.22
	3	Re	0	1	13.07	−15.97	63.24	−9.28	36.76	−0.22	−11.95
	4	Os	1	0	19.23	−11.44	38.77	−18.07	61.23	−0.27	−10.55
	5	Ir	0	1	18.13	−19.08	61.46	−11.96	38.54	−0.25	−13.17
	6	Pt	0	1	18.24	−19.97	62.12	−12.18	37.88	−0.17	−14.09
1,4-*carbo*-bimetallic	7	Ru	2	0	36.90	−18.10	39.82	−27.30	60.18	−0.50	−9.03
	8	Os	2	0	21.60	−14.50	43.50	−18.80	56.50	−0.30	−12.00
	9	Ir	0	1	24.20	−20.30	53.99	−17.30	46.01	−0.30	−13.70
	10	Pt	0	1	17.30	−16.10	51.41	−15.20	48.59	−0.20	−14.20
1,7-*carbo*-bimetallic	11	Ru	2	0	14.40	−7.00	39.13	−10.89	60.87	−0.35	−3.84
	12	Rh	0	1	15.62	−15.57	58.31	−11.13	41.69	−0.31	−11.39
	13	Re	0	1	12.20	−14.50	60.99	−9.28	39.01	−0.20	−11.80
	14	Os	2	0	18.10	−10.10	37.92	−16.50	62.08	−0.30	−8.75
	15	Ir	0	1	17.90	−18.50	60.01	−12.30	39.99	−0.30	−13.10
	16	Pt	0	1	26.00	−22.80	56.93	−17.20	43.07	−0.20	−14.20
1,10-*carbo*-bimetallic	17	Ru	2	0	16.20	−11.90	43.88	−15.20	56.12	−0.20	−11.10
	18	Rh	0	1	15.60	−16.50	60.60	−10.70	39.40	−0.30	−8.59
	19	Re	0	1	12.80	−15.40	62.61	−9.18	37.39	−0.20	−11.90
	20	Os	2	0	19.40	−14.20	45.05	−17.30	54.95	−0.30	−12.30
	21	Ir	0	1	20.00	−19.80	58.26	−14.20	41.74	−0.20	−14.20
	22	Pt	0	1	18.20	−20.00	60.09	−13.30	39.91	−0.20	−15.30

[a]Energies are collected in eV.

Figure 13. Electron delocalization for system **6** in the (left) $EDDB_G$ function and (right) $EDDB_P$ function. Isovalue = 0.01.

atoms and the contribution per carbon atom was significatively reduced. Except for osmium systems **4** and **20** with metal contributions of 0.58e and 0.83e, respectively.

While all systems presented a partially delocalized electron nature, some of them could be potentially aromatic based on the low change in the population per carbon atom (systems **3** and **6**), and the total electron population delocalization. If the total delocalized electron population was applied to the Hückel's rule, then, the *carbo*-benzene would be an aromatic system with $n = 3$, while if $n = 2$ is considered (total electrons equals 10), then system **2** with a total population of 10.39e, system **5** with 9.45e, system **10** with 9.83e, system **13** with 9.57e, and system **16** with 9.76e were potentially aromatic systems. Alongside system **15** with $n = 1$ (total electrons equals 6) and a total population of 5.95e, system **20** with 6.31e.

3.3. Electronic Delocalization. *3.3.1. Magnetically Induced Current Density.* The four-component Dirac Hamil-

https://doi.org/10.1021/acsomega.3c10049
ACS Omega 2024, 9, 10913−10928

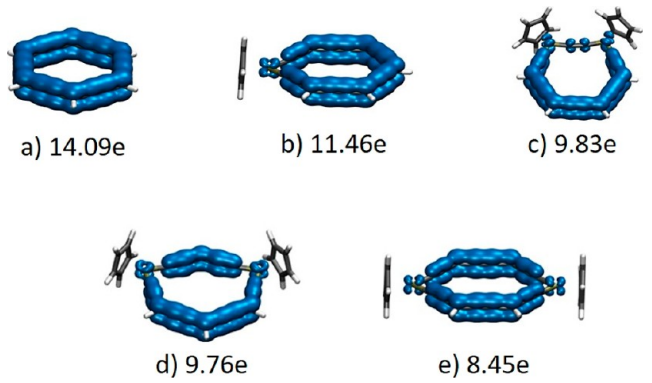

Figure 14. EDDB$_P$ for (a) *carbo*-benzene, (b) system **6**, (c) system **10**, (d) system **16**, and (e) system **22**. Isovalue = 0.01.

tonian was used to compute the induced current density. The relativistic current density is plotted at the molecular plane, and at the planes at $1a_0$ and $2a_0$ above the ring. As a reference, the carbomer molecule is plotted (Figure 15). The delocalized nature of the carbomer system was more evident at $1a_0$ and $2a_0$ over the molecular plane. Diatropic current densities were induced in a counterclockwise direction over the carbons, and in the inner part of the ring, a paratropic current density was sustained. This behavior was analogous to the benzene molecule and then it could be categorized as aromatic[16] based on this magnetic criterion.

This behavior was also found in some system proposed here. Systems **2**, **3**, **5**, **6**, **9**, **10**, **16**, **15**, and **22** could be considered aromatic, they could sustain diatropic currents at different levels. Figure 16 shows the plots where the diatropic current is highlighted in the possible aromatic systems. Blue arrows represent total diatropic current, while the green arrow represents local diatropic currents. The integration of the current densities was not calculated due to important statements: (i) the local diatropic response contributes to the total diatropic response. This contribution influences the integration of the current density possibly overestimating the total diatropic current density. (ii) The integration is path-dependent and there was not a common integration plane. The closer to a nucleus the path is, the bigger the integrated value will result. This also occur if the plane contains a considerable amount of local current densities. (iii) The lack of symmetry of the system results of different values if it is integrated in different directions, i.e., above or below the molecular plane.

3.3.2. Induced Magnetic Field, B^{ind}. The $\mathbf{B}^{ind}$ is a vector that represents the magnetic response of the molecules exposed to an external magnetic field ($\mathbf{B}^{ext}$). The *z*-component of this vector is labeled as B_z^{ind}, and it is equivalent to the negative of the zz-component of the shielding tensor (and also equivalent to NICS$_{zz}$). B_z^{ind} is a scalar value and it was calculated in several points placed perpendicular to the molecular ring (Scheme 6).[59,60] This induced field is characteristic for antiaromatic and aromatic molecules and, the more negative is the value of B_z^{ind}, more diatropic the system is. For a better reference, the B_z^{ind} of *carbo*-benzene and *iminobora*-borazine were also computed. Only planar or quasi-planar molecules were analyzed with this methodology.

The first group analyzed was the monosubstituted and the magnetic response of **1**, **2**, and **4** was similar to the response of *iminobora*-borazine (see Figure 17). For this reason, they could be catalogued as no-aromatic. However, the diatropic responses of **5** and **6** were less intense than *carbo*-benzene but they could be catalogued as aromatic.

Compounds with a double metallic center were separated in the 1,4-, 1,7-, and 1,10-*carbo*-mer groups (Figure 18). Following this order, the first analyzed group was the 1,4-*carbo*-mers. For this group, **7** was not analyzed due its nonplanar geometry. The magnetic response of **8** is similar in distribution and magnitude to the response calculated in the *iminobora*-borazine. The other two rings, **9** and **10**, presented a diatropic response. The magnetic responses of the rings with 1,7-orientation, **14**, **15**, and **16**, showed a no-aromatic character due to the weak diatropic response. In particular, the response of **14** was equivalent to the *iminobora*-borazine. Finally, the set conformed by the 1,10-*carbo*-mer rings, **20** could be catalogued as no-aromatic; and **19**, **21** and **22** could be considered as aromatic compounds, but not comparable with the diatropic response of the *carbo*-benzene.

In general, the inclusion of the metallic centers in the *carbo*-benzene ring generated a diminished intensity of the diatropic character. Also, the nonfully delocalized compounds (**8**, **14**, and **20**) presented a similar magnetic response to *iminobora*-borazine, for this reason, they could be catalogued as no-aromatic.

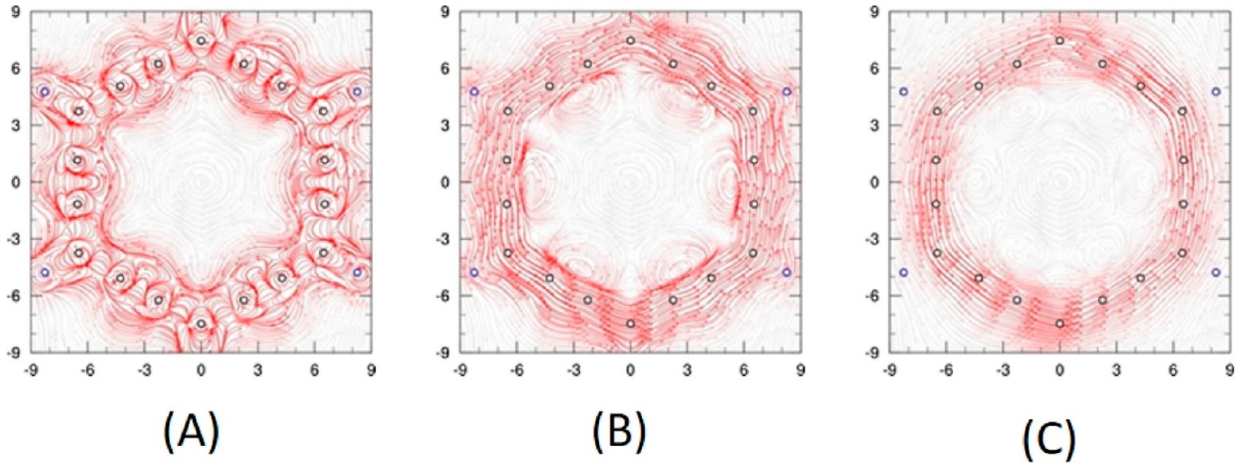

Figure 15. MICD with four-component Dirac Hamiltonian for *carbo*-benzene system. (A) At the molecular plane, (B) at $1a_0$ above the molecular plane, and (C) $2a_0$ above the molecular plane. Counterclockwise direction represents diatropic current (aromatic).

https://doi.org/10.1021/acsomega.3c10049
ACS Omega 2024, 9, 10913−10928

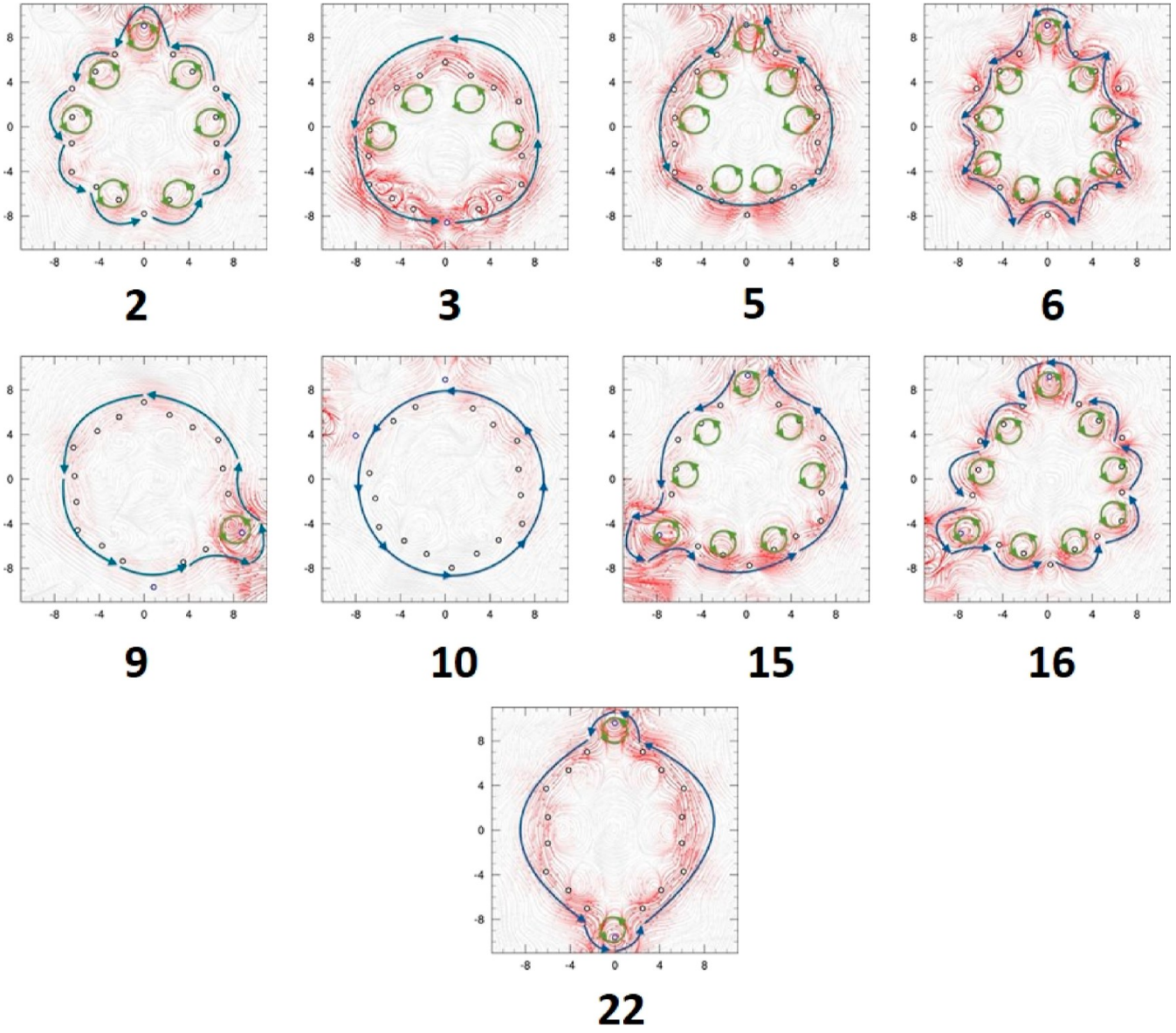

Figure 16. MICD for aromatic systems. Blue arrows belong to total current density and the green arrow to local current density.

When the profiles were grouped by element instead of oriented-substitution, it was possible to observe that osmium's *carbo*-mers presented a paratropic values with values around 4 ppm around the ring's center, except for **4** which was around −4 ppm in the same zone. The *carbomers* formed with iridium and platinum could be catalogued as (slightly) diatropic compounds based on their magnetic response. The *carbo*-mers of ruthenium and rhenium were not analyzed in all the conformations. Plots formed by the profiles of B_z^{ind} grouped by element are depicted in the Supporting Information.

In Figure 19, isolines maps and isosurfaces of the B_z^{ind} calculated in *carbo*-benzene, *iminobora*-borazine, and the platinum rings (**6**, **10**, **16**, and **22**) are depicted (isolines maps of all the rings are reported in the Supporting Information). Compared with *carbo*-benzene, the rest of the rings presented a smaller diatropic response or, in other words, they were less aromatic. As expected, the electronic delocalization in *iminobora*-borazine was interrupted by the difference of the electronegativities of the boron and nitrogen atoms, generating strong diatropic zones around the nitrogen atoms, generating a characteristic response associated to a no-aromatic molecule.

4. CONCLUSIONS

The configurations of *carbo*-metallabenzenes and *carbo*-dimatellabenzenes generally maintained carbon−carbon bond lengths akin to those observed in *carbo*-benzene. Despite a discernible reduction in electronic delocalization resulting from the introduction of metallic centers, the distribution pattern of their impact within the ring structure exhibited no consistent trend. Notably, the specific metallic atoms selected played a decisive role in influencing electronic delocalization, with platinum and iridium compounds demonstrating the highest degree of delocalization. Osmium-containing rings exhibited responses comparable to those observed in *iminobora*-borazine.

In terms of the most stable isomer, only osmium, iridium, and platinum exhibited comparability, as they were the sole elements yielding planar (or quasi-planar) rings across all three proposed orientations for *carbo*-dimatellabenzenes. Remarkably, the 1,10-*carbo*-mers rings did not emerge as the most

https://doi.org/10.1021/acsomega.3c10049
ACS Omega 2024, 9, 10913−10928

Scheme 6. Orientation of the Profile Computed in the *Carbo*-Cycles[a]

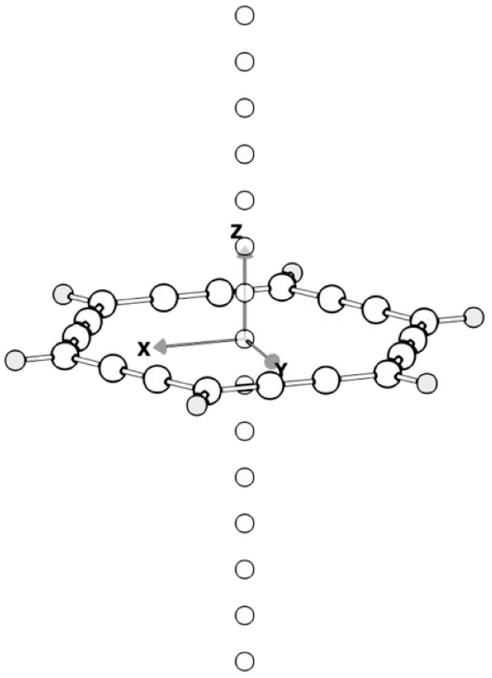

[a]The shielding tensors were computed perpendicular to the molecular plane and parallel to the *z*-axis.

stable or aromatic. For iridium and platinum, the 1,7-*carbo*-mers configurations proved to be the most stable, deviating from the anticipated trend. However, only 1,7-*carbo*-diiridiumbenzene adhered to the expectation that the most aromatic isomer corresponds to the most stable. Finally, a comprehensive summary of the aromaticity analysis results is presented in Table 3.

■ ASSOCIATED CONTENT

Supporting Information

The Supporting Information is available free of charge at https://pubs.acs.org/doi/10.1021/acsomega.3c10049.

MO diagrams of the complete series of systems, EDDB figures, MICD figures separated by a metallic center, B_z^{ind}

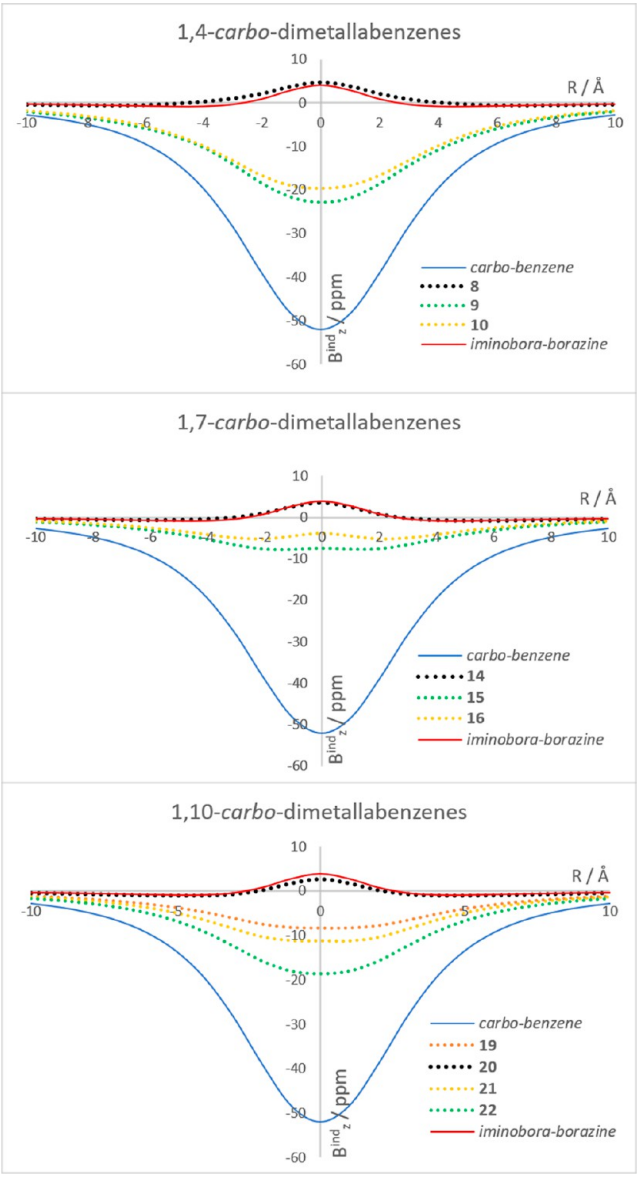

Figure 18. Profiles of the B_z^{ind} computed on *carbo*-dimetallabenzenes, including *carbo*-benzene and iminobora-borazine as reference.

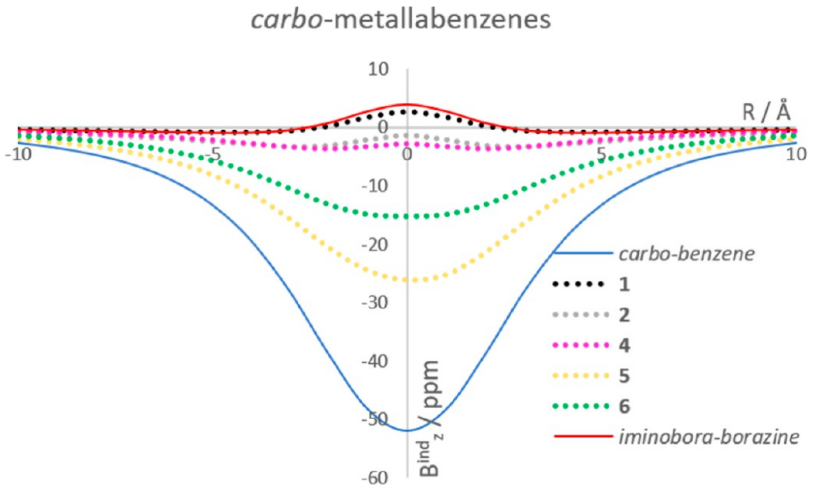

Figure 17. Profile of the B_z^{ind} computed on *carbo*-metallabenzenes, including *carbo*-benzene and *iminobora*-borazine as reference.

https://doi.org/10.1021/acsomega.3c10049
ACS Omega 2024, 9, 10913−10928

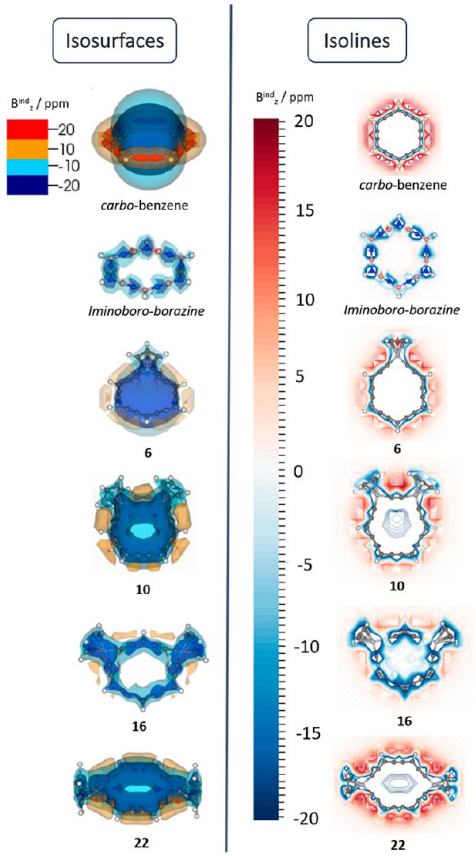

Figure 19. Isolines maps and isosurfaces of the B_z^{ind} calculated in *carbo*-benzene, *iminobora*-borazine, and platinum rings. Isolines maps are placed.

profiles grouped by the metallic center, and B_z^{ind} isolines of all the proposed molecules (PDF)

AUTHOR INFORMATION

Corresponding Authors

David Arias-Olivares − *Center of Applied Nanoscience (CANS), Facultad de Ciencias Exactas, Universidad Andres Bello, Santiago 8370146, Chile;* orcid.org/0000-0002-1701-8288; Email: ndariaso@gmail.com

Rafael Islas − *Departamento de Ciencias Químicas, Facultad de Ciencias Exactas and Centro de Química Teórica & Computacional (CQT&C), Facultad de Ciencias Exactas, Universidad Andres Bello, Santiago 8370146, Chile;* orcid.org/0000-0001-5655-107X; Email: rafael.islas@unab.cl

Authors

Andrés Becerra-Buitrago − *Doctorado en Fisicoquímica Molecular, Facultad de Ciencias Exactas, Universidad Andres Bello, Santiago 8370146, Chile;* orcid.org/0000-0003-4962-9603

Luis Carlos García-Sánchez − *Proyecto Curricular Licenciatura en Química, Universidad Distrital Francisco José de Caldas, Bogotá 11021-110231588, Colombia*

Diego V. Moreno − *Programa de Química, Universidad de Ciencias Aplicadas y Ambientales, Bogotá 6684700, Colombia*

Complete contact information is available at: https://pubs.acs.org/10.1021/acsomega.3c10049

Table 3. Final Summary of the Analysis of Aromaticity

system	metal	charge	EDDB	MICD	B_z^{ind}
1	Ru	1	delocalized[a]	no delocalized	low diatropic[d]
2	Rh	0	delocalized[a]	low delocalized	low diatropic[d]
3	Re	0	delocalized[a]	half delocalized	no analyzed[b]
4	Os	1	delocalized[a]	no delocalized	low diatropic[d]
5	Ir	0	delocalized[a]	delocalized	diatropic[c]
6	Pt	0	delocalized[a]	delocalized	diatropic[c]
7	Ru	2	half delocalized[a]	half delocalized	no analyzed[b]
8	Os	2	half delocalized[a]	half delocalized	low diatropic[d]
9	Ir	0	half delocalized[a]	delocalized	diatropic[c]
10	Pt	0	half delocalized[a]	delocalized	diatropic[c]
11	Ru	2	half delocalized	half delocalized	no analyzed[b]
12	Rh	0	half delocalized[a]	half delocalized	no analyzed[b]
13	Re	0	delocalized[a]	not analyzed[a]	no analyzed[b]
14	Os	2	delocalized[e]	no delocalized	low diatropic[d]
15	Ir	0	half delocalized[a]	delocalized	low diatropic
16	Pt	0	delocalized[a]	delocalized	low diatropic
17	Ru	2	half delocalized[a]	no delocalized	low diatropic[d]
18	Rh	0	half delocalized[a]	half delocalized	no analyzed[b]
19	Re	0	delocalized[a]	not analyzed	low diatropic
20	Os	2	half delocalized[a]	no delocalized	low diatropic[d]
21	Ir	0	half delocalized[a]	not analyzed[e]	low diatropic
22	Pt	0	delocalized[a]	delocalized	diatropic[c]

[a]Observations: the ring is delocalized except for the metallic center. [b]No planar ring. [c]Less diatropic than *carbo*-benzene. [d]Magnetic response similar to inorganic iminobora-borazine. Associated to the nonaromatic response. [e]Unstable obtained wave function.

Notes

The authors declare no competing financial interest.

ACKNOWLEDGMENTS

L.C.G.-S. and A.B.-B. acknowledge the CECAD-UD for the Computing Facility and CIDC for the financial support under the project 4-50-598-19.

REFERENCES

(1) Thorn, D. L.; Hoffmann, R. Delocalization in metallocycles. *Nouv. J. Chim.* **1979**, *3* (1), 39−45.

(2) Elliott, G. P.; Roper, W. R.; Waters, J. M. Metallacyclohexatrienes or 'metallabenzenes.' Synthesis of osmabenzene derivatives and X-ray crystal structure of [Os(CSCHCHCHCH)(CO)(PPh3)2]. *J. Chem. Soc., Chem. Commun.* **1982**, No. 14, 811−813.

(3) Bleeke, J. R. Metallabenzenes. *Chem. Rev.* **2001**, *101* (5), 1205−1228.

(4) Masui, H. Metalloaromaticity. *Coord. Chem. Rev.* **2001**, *219−221*, 957−992.

(5) Calvin, M.; Wilson, K. W. Stability of Chelate Compounds. *J. Am. Chem. Soc.* **1945**, *67* (11), 2003−2007.

(6) Fernández, I.; Frenking, G.; Merino, G. Aromaticity of metallabenzenes and related compounds. *Chem. Soc. Rev.* **2015**, *44* (18), 6452−6463.

https://doi.org/10.1021/acsomega.3c10049
ACS Omega 2024, 9, 10913−10928

(7) Schleyer, P. v. R.; Pühlhofer, F. Recommendations for the Evaluation of Aromatic Stabilization Energies. *Org. Lett.* **2002**, *4* (17), 2873−2876.
(8) De Proft, F.; Geerlings, P. Relative hardness as a measure of aromaticity. *Phys. Chem. Chem. Phys.* **2004**, *6* (2), 242−248.
(9) Lin, R.; Lee, K.-H.; Poon, K. C.; Sung, H. H. Y.; Williams, I. D.; Lin, Z.; Jia, G. Synthesis of Rhenabenzenes from the Reactions of Rhenacyclobutadienes with Ethoxyethyne. *Chem. - Eur. J.* **2014**, *20* (45), 14885−14899.
(10) Ishii, T.; Suzuki, K.; Nakamura, T.; Yamashita, M. An Isolable Bismabenzene: Synthesis, Structure, and Reactivity. *J. Am. Chem. Soc.* **2016**, *138* (39), 12787−12790.
(11) Iron, M. A.; Lucassen, A. C. B.; Cohen, H.; van der Boom, M. E.; Martin, J. M. L. A Computational Foray into the Formation and Reactivity of Metallabenzenes. *J. Am. Chem. Soc.* **2004**, *126* (37), 11699−11710.
(12) Chen, J.; Shi, C.; Sung, H. H. Y.; Williams, I. D.; Lin, Z.; Jia, G. Synthesis and Characterization of Rhenabenzyne Complexes. *Chem. - Eur. J.* **2012**, *18* (44), 14128−14139.
(13) Schleyer, P. v. R.; Maerker, C.; Dransfeld, A.; Jiao, H. J.; van Eikema Hommes, N. J. R. Nucleus-independent chemical shifts: A simple and efficient aromaticity probe. *J. Am. Chem. Soc.* **1996**, *118* (26), 6317−6318.
(14) Chen, Z.; Wannere, C. S.; Corminboeuf, C.; Puchta, R.; Schleyer, P. v. R. Nucleus-Independent Chemical Shifts (NICS) as an Aromaticity Criterion. *Chem. Rev.* **2005**, *105* (10), 3842−3888.
(15) Islas, R.; Heine, T.; Merino, G. The Induced Magnetic Field. *Acc. Chem. Res.* **2012**, *45* (2), 215−228.
(16) Arias-Olivares, D.; Becerra-Buitrago, A.; García-Sánchez, L. C.; Islas, R. In Silico Analysis of the Electronic Delocalization in Some Double Fused-Ring Metallabenzenes. *ACS Omega* **2021**, *6* (14), 9887−9897.
(17) Islas, R.; Arias-Olivares, D.; Becerra-Buitrago, A.; García-Sánchez, L. C.; Méndez-Ayón, L. N.; Zuniga-Gutierrez, B. Metallaborazines: To Be or Not To Be Delocalized. *ACS Omega* **2021**, *6* (30), 19629−19641.
(18) Islas, R.; Poater, J.; Solà, M. Analysis of the Aromaticity of Five-Membered Heterometallacycles Containing Os, Ru, Rh, and Ir. *Organometallics* **2014**, *33* (7), 1762−1773.
(19) Vásquez-Espinal, A.; Poater, J.; Solà, M.; Tiznado, W.; Islas, R. Testing the effectiveness of the isoelectronic substitution principle through the transformation of aromatic osmathiophene derivatives into their inorganic analogues. *New J. Chem.* **2017**, *41* (3), 1168−1178.
(20) Chen, D.; Hua, Y.; Xia, H. Metallaaromatic Chemistry: History and Development. *Chem. Rev.* **2020**, *120* (23), 12994−13086.
(21) Chauvin, R. Carbomers. I. A general concept of expanded molecules. *Tetrahedron Lett.* **1995**, *36* (3), 397−400.
(22) Chauvin, R. Carbomers. II. En route to [C,C]6carbo-benzene. *Tetrahedron Lett.* **1995**, *36* (3), 401−404.
(23) Maraval, V.; Chauvin, R. From Macrocyclic Oligo-acetylenes to Aromatic Ring Carbo-mers. *Chem. Rev.* **2006**, *106* (12), 5317−5343.
(24) Islas, R.; Oyarzún, D. P.; Cantero-López, P. Analysis of the aromaticity in extended systems formed from isoelectronic Al42- and C42+ aromatic clusters. *Struct. Chem.* **2018**, *29* (5), 1383−1395.
(25) Jalife, S.; Audiffred, M.; Islas, R.; Escalante, S.; Pan, S.; Chattaraj, P. K.; Merino, G. The inorganic analogues of carbo-benzene. *Chem. Phys. Lett.* **2014**, *610*−*611*, 209−212.
(26) Azpiroz, J. M.; Islas, R.; Moreno, D.; Fernández-Herrera, M. A.; Pan, S.; Chattaraj, P. K.; Martínez-Guajardo, G.; Ugalde, J. M.; Merino, G. Carbo-Cages: A Computational Study. *J. Org. Chem.* **2014**, *79* (12), 5463−5470.
(27) Poater, J.; Heitkämper, J.; Poater, A.; Maraval, V.; Chauvin, R. Zwitterionic Aromaticity on Azulene Extrapolated to carbo-Azulene. *Eur. J. Org Chem.* **2021**, *2021* (46), 6450−6458.
(28) Lepetit, C.; Godard, C.; Chauvin, R. Aromaticity and homoaromaticity of annulene ring carbomers. *New J. Chem.* **2001**, *25* (4), 572−580.
(29) Cocq, K.; Lepetit, C.; Maraval, V.; Chauvin, R. Carbo-aromaticity" and novel carbo-aromatic compounds. *Chem. Soc. Rev.* **2015**, *44* (18), 6535−6559.
(30) Saccavini, C.; Sui-Seng, C.; Maurette, L.; Lepetit, C.; Soula, S.; Zou, C.; Donnadieu, B.; Chauvin, R. Functional [6]Pericyclynes: Aromatization to Substituted carbo-Benzenes. *Chem. - Eur. J.* **2007**, *13* (17), 4914−4931.
(31) Zou, C.; Lepetit, C.; Coppel, Y.; Chauvin, R. Ring carbo-mers: From questionable homoaromaticity to bench aromaticity. *Pure Appl. Chem.* **2006**, *78* (4), 791−811.
(32) Tanimoto, H.; Fujiwara, T.; Mori, J.; Nagao, T.; Nishiyama, Y.; Morimoto, T.; Ito, S.; Tanaka, K.; Chujo, Y.; Kakiuchi, K. Extended germa[N]pericyclynes: synthesis and characterization. *Dalton Trans.* **2017**, *46* (7), 2281−2288.
(33) Perdew, J. P.; Burke, K.; Ernzerhof, M. Generalized Gradient Approximation Made Simple. *Phys. Rev. Lett.* **1996**, *77* (18), 3865−3868.
(34) Perdew, J. P.; Burke, K.; Ernzerhof, M. Generalized Gradient Approximation Made Simple [Phys. Rev. Lett. 77, 3865 (1996)]. *Phys. Rev. Lett.* **1997**, *78* (7), 1396.
(35) Adamo, C.; Barone, V. Toward reliable density functional methods without adjustable parameters: The PBE0 model. *J. Chem. Phys.* **1999**, *110* (13), 6158−6170.
(36) Van Lenthe, E.; Baerends, E. J. Optimized Slater-type basis sets for the elements 1−118. *J. Comput. Chem.* **2003**, *24* (9), 1142−1156.
(37) Rolfes, J. D.; Neese, F.; Pantazis, D. A. All-electron scalar relativistic basis sets for the elements Rb-Xe. *J. Comput. Chem.* **2020**, *41* (20), 1842−1849.
(38) Neese, F.; Wennmohs, F.; Becker, U.; Riplinger, C. The ORCA quantum chemistry program package. *J. Chem. Phys.* **2020**, *152* (22), 224108.
(39) Neese, F. Software update: The ORCA program system—Version 5.0. *Wiley Interdiscip. Rev.: Comput. Mol. Sci.* **2022**, *12* (5), No. e1606.
(40) Michalak, A.; DeKock, R. L.; Ziegler, T. Bond Multiplicity in Transition-Metal Complexes: Applications of Two-Electron Valence Indices. *J. Phys. Chem. A* **2008**, *112* (31), 7256−7263.
(41) Mitoraj, M. P.; Michalak, A.; Ziegler, T. A Combined Charge and Energy Decomposition Scheme for Bond Analysis. *J. Chem. Theory Comput.* **2009**, *5* (4), 962−975.
(42) Szczepanik, D. W.; Andrzejak, M.; Dominikowska, J.; Pawełek, B.; Krygowski, T. M.; Szatylowicz, H.; Solà, M. The electron density of delocalized bonds (EDDB) applied for quantifying aromaticity. *Phys. Chem. Chem. Phys.* **2017**, *19* (42), 28970−28981.
(43) Shavitt, I. *Methods of Electronic Structure Theory*; Modern Theoretical Chemistry; Springer, 1977.
(44) Wadt, W. R.; Hay, P. J. Ab initio effective core potentials for molecular calculations. Potentials for main group elements Na to Bi. *J. Chem. Phys.* **1985**, *82* (1), 284−298.
(45) Frisch, M. J.; Trucks, G. W.; Schlegel, H. B.; Scuseria, G. E.; Robb, M. A.; Cheeseman, J. R.; Scalmani, G.; Barone, V.; Petersson, G. A.; Nakatsuji, H.; Li, X.; Caricato, M.; Marenich, A. V.; Bloino, J.; Janesko, B. G.; Gomperts, R.; Mennucci, B.; Hratchian, H. P.; Ortiz, J. V.; Izmaylov, A. F.; Sonnenberg, J. L.; Williams; Ding, F.; Lipparini, F.; Egidi, F.; Goings, J.; Peng, B.; Petrone, A.; Henderson, T.; Ranasinghe, D.; Zakrzewski, V. G.; Gao, J.; Rega, N.; Zheng, G.; Liang, W.; Hada, M.; Ehara, M.; Toyota, K.; Fukuda, R.; Hasegawa, J.; Ishida, M.; Nakajima, T.; Honda, Y.; Kitao, O.; Nakai, H.; Vreven, T.; Throssell, K.; Montgomery, J. A., Jr.; Peralta, J. E.; Ogliaro, F.; Bearpark, M. J.; Heyd, J. J.; Brothers, E. N.; Kudin, K. N.; Staroverov, V. N.; Keith, T. A.; Kobayashi, R.; Normand, J.; Raghavachari, K.; Rendell, A. P.; Burant, J. C.; Iyengar, S. S.; Tomasi, J.; Cossi, M.; Millam, J. M.; Klene, M.; Adamo, C.; Cammi, R.; Ochterski, J. W.; Martin, R. L.; Morokuma, K.; Farkas, O.; Foresman, J. B.; Fox, D. J. *Gaussian 16* Rev. B.01: Wallingford, CT, 2016.
(46) Elvidge, J. A.; Jackman, L. M. 181. Studies of aromaticity by nuclear magnetic resonance spectroscopy. Part I. 2-Pyridones and related systems. *J. Chem. Soc.* **1961**, No. 0, 859−866.

https://doi.org/10.1021/acsomega.3c10049
ACS Omega 2024, 9, 10913−10928

(47) Saue, T.; Jensen, H. J. A. Linear response at the 4-component relativistic level: Application to the frequency-dependent dipole polarizabilities of the coinage metal dimers. *J. Chem. Phys.* **2003**, *118* (2), 522−536.
(48) PyNGL; National Center for Atmospheric Research, 2019, http://www.pyngl.ucar.edu/.
(49) Visscher, L.; H. J. A., Jensen; Bast, R.; Saue, T.; with contributions from Bakken, V.; Dyall, K. G.; Dubillard, S.; Ekström, U.; Eliav, E.; Enevoldsen, T.; Faßhauer, E.; Fleig, T.; Fossgaard, O.; Gomes, A. S. P.; Hedegård, E. D.; Helgaker, T.; Henriksson, J.; Iliaš, M.; Jacob, Ch. R.; Knecht, S.; Komorovský, S.; Kullie, O.; Lærdahl, J. K.; Larsen, C. V.; Lee, Y. S.; Nataraj, H. S.; Nayak, M. K.; Norman, P.; Olejniczak, G.; Olsen, J.; Olsen, J. M. H.; Park, Y. C.; Pedersen, J. K.; Pernpointner, M.; Di Remigio, R.; Ruud, K.; Sałek, P.; Schimmelpfennig, B.; Shee, A.; Sikkema, J.; Thorvaldsen, A. J.; Thyssen, J.; Stralen, J. v.; Villaume; Visser, O.; Winther, T.; Yamamoto, S. *DIRAC, a Relativistic Ab Initio Electronic Structure Program, Release DIRAC17* see http://www.diracprogram.org 2017.
(50) Bast, R.; Jusélius, J.; Saue, T. 4-Component relativistic calculation of the magnetically induced current density in the group 15 heteroaromatic compounds. *Chem. Phys.* **2009**, *356* (1−3), 187−194.
(51) Dunning, T. H., Jr. Gaussian basis sets for use in correlated molecular calculations. I. The atoms boron through neon and hydrogen. *J. Chem. Phys.* **1989**, *90* (2), 1007−1023.
(52) Dyall, K. G.; Gomes, A. S. P. Revised relativistic basis sets for the 5d elements Hf-Hg. *Theor. Chem. Acc.* **2010**, *125* (1−2), 97−100.
(53) Weigend, F.; Ahlrichs, R. Balanced basis sets of split valence, triple zeta valence and quadruple zeta valence quality for H to Rn: Design and assessment of accuracy. *Phys. Chem. Chem. Phys.* **2005**, *7* (18), 3297−3305.
(54) Andrae, D.; Haeussermann, U.; Dolg, M.; Stoll, H.; Preuss, H. Energy-adjusted ab initio pseudopotentials for the second and third row transition elements. *Theor. Chim. Acta* **1990**, *77*, 123−141.
(55) Pritchard, B. P.; Altarawy, D.; Didier, B.; Gibson, T. D.; Windus, T. L. New Basis Set Exchange: An Open, Up-to-Date Resource for the Molecular Sciences Community. *J. Chem. Inf. Model.* **2019**, *59* (11), 4814−4820.
(56) Qin, X.; Zhou, Q.; Chen, Z.-N.; Zhang, L. Understanding and Designing of Bent Aromatic Heterometallabenzenes. *Organometallics* **2023**, *42* (15), 2148−2158.
(57) Zhu, J.; Jia, G.; Lin, Z. Understanding Nonplanarity in Metallabenzene Complexes. *Organometallics* **2007**, *26* (8), 1986−1995.
(58) Rzepa, H. S. A Double-Twist Möbius-Aromatic Conformation of [14]Annulene. *Org. Lett.* **2005**, *7* (21), 4637−4639.
(59) Morao, I.; Cossio, F. P. A simple ring current model for describing in-plane aromaticity in pericyclic reactions. *J. Org. Chem.* **1999**, *64* (6), 1868−1874.
(60) Jusélius, J.; Sundholm, D. Ab initio determination of the induced ring current in aromatic molecules. *Phys. Chem. Chem. Phys.* **1999**, *1* (15), 3429−3435.

https://doi.org/10.1021/acsomega.3c10049
ACS Omega 2024, 9, 10913−10928